

RELATIVISTIC SIMULATIONS OF BLACK HOLE–NEUTRON STAR COALESCENCE: THE JET EMERGES

VASILEIOS PASCHALIDIS^{1,2}, MILTON RUIZ², STUART L. SHAPIRO^{2,3}

¹Department of Physics, Princeton University, Princeton, NJ 08544

²Department of Physics, University of Illinois at Urbana-Champaign, Urbana, IL 61801

³Department of Astronomy & NCSA, University of Illinois at Urbana-Champaign, Urbana, IL 61801

Draft version June 11, 2015

ABSTRACT

We perform magnetohydrodynamic simulations in full general relativity (GRMHD) of a binary black hole–neutron star on a quasicircular orbit that undergoes merger. The binary mass ratio is 3 : 1, the black hole initial spin parameter $a/m = 0.75$ (m is the black hole Christodoulou mass) aligned with the orbital angular momentum, and the neutron star is an irrotational $\Gamma = 2$ polytrope. About two orbits prior to merger (at time $t = t_B$), we seed the neutron star with a dynamically weak interior dipole magnetic field that extends into the stellar exterior. At $t = t_B$ the exterior has a low-density atmosphere with constant plasma parameter $\beta \equiv P_{\text{gas}}/P_{\text{mag}}$. Varying β at t_B in the exterior from 0.1 to 0.01, we find that at a time $\sim 4000M \sim 100(M_{\text{NS}}/1.4M_{\odot})\text{ms}$ [M is the total (ADM) mass] following the onset of accretion of tidally disrupted debris, magnetic winding above the remnant black hole poles builds up the magnetic field sufficiently to launch a mildly relativistic, collimated outflow – an incipient jet. The duration of the accretion and the lifetime of the jet is $\Delta t \sim 0.5(M_{\text{NS}}/1.4M_{\odot})\text{s}$. Our simulations furnish the first explicit examples in GRMHD which show that a jet can emerge following a black hole – neutron star merger.

Subject headings: black hole physics—gamma-ray burst: general—gravitation—gravitational waves—stars: neutron

1. INTRODUCTION

Black hole–neutron star (BHNS) binaries are promising sources for detectable gravitational waves (GWs) by ground-based laser interferometers such as aLIGO (Brown et al. 2004), VIRGO (Acernese & the VIRGO Collaboration 2006), GEO (Lück & the GEO600 collaboration 2006), and KAGRA (Kuroda & LCGT Collaboration 2010). Moreover, mergers of BHNSs have been suggested as central engines that power short-hard gamma ray bursts (sGRBs); see, e.g., (Meszaros 2006; Lee & Ramirez-Ruiz 2007). The GW signal from the inspiral and merger, the amount and composition of ejecta from BHNSs and effects of different equations of state (EOS), have been explored in full general relativity (GR) (see, e.g. Etienne et al. 2009; Duez et al. 2010; Shibata & Taniguchi 2011; East et al. 2012; Lovelace et al. 2013; Lackey et al. 2014; Kyutoku et al. 2013; Deaton et al. 2013; Pannarale et al. 2013; Tanaka et al. 2014; Foucart et al. 2014). Studies of magnetized BHNS mergers in full GR magnetohydrodynamics (MHD) also have been carried out (Chawla et al. 2010; Etienne et al. 2012a,b). Magnetospherically-powered precursor EM signals from BHNS systems have been simulated as well (Paschalidis et al. 2013).

While these studies have made great progress, to date, there exists no self-consistent calculation in full GR that starts from the late BHNS inspiral and demonstrates that jets can be launched from BHNSs. This step is crucial to establishing BHNSs as viable central engines for sGRBs and solidifying their role as multimessenger systems.

It is known that if the initial NS has a B field confined to its interior, the B-field lines following the BHNS merger are wound into an almost purely toroidal configuration and no jets are launched (Etienne et al. 2012a,b). The existence of near purely toroidal B fields in the rem-

nant disk explains why jets cannot be launched magnetically: for a magnetized accretion disk with B fields initially confined to the disk interior, a jet is launched and supported only if these initial seed fields have poloidal components with a consistent sign in the vertical direction (Beckwith et al. 2008). Applying this principle, we demonstrated that by artificially seeding with a purely poloidal B field the remnant disk formed in a hydrodynamic simulation of a BHNS merger, an incipient jet is indeed launched (Etienne et al. 2012b). Thus, under “right conditions,” jets can be magnetically launched from BHNSs. However, identifying the initial configuration prior to tidal disruption that leads to these “right conditions” remains elusive. We note that there exists a calculation for binary NSs that reports jet formation (Rezzolla et al. 2011), but a more recent high-resolution study (Kiuchi et al. 2014) suggests otherwise.

In these early GRMHD BHNS studies, the B fields were confined to the NS interior. However, NSs are expected to be endowed with dipole B fields that extend into the NS exterior (as is required by pulsars). A more realistic initial configuration for a magnetized BHNS merger should contain a NS endowed with a dipolar B field extending from the NS interior well into the exterior. Two new features then arise: (1) poloidal B-field lines attached to fluid elements thread the BH prior to tidal disruption, and (2) following disruption, while the B field in the disk remains predominantly toroidal, the initially poloidal B field in the exterior maintains a strong poloidal component threading the low-density debris (see Figure 1).

Motivated by these considerations, we perform ideal GRMHD simulations of BHNS systems and show that they can launch incipient jets if the NS is initially endowed with a dipolar B field extending into the exterior.

TABLE 1
SUMMARY OF RESULTS

β_0	Γ_L ^a	$\dot{M}(M_\odot \text{ s}^{-1})$ ^b	$M_{\text{disk}}/M_{\text{NS}}$	α -stress	L_{EM} ^c
0.01	1.25	0.25	9.9%	0.01-0.03	1.5×10^{51}
0.05	1.3	0.39	9.1%	0.015-0.035	5.4×10^{51}
0.1	1.2	0.31	9.4%	0.02-0.04	0.9×10^{51}

^a Maximum fluid Lorentz factor near the end of the simulation.

^b Rest-mass accretion rate when the outflow reaches $100M = 758(M_{\text{NS}}/1.4M_\odot)$ km above the BH poles.

^c Outgoing Poynting luminosity in units of erg s^{-1} , time-averaged over the last $1000M = 25(M_{\text{NS}}/1.4M_\odot)$ ms of the evolution, after the jet is well-developed.

We use geometrized units, $G = c = 1$.

2. METHODS

We carry out the simulations employing the Illinois GRMHD adaptive-mesh refinement code, which adopts the *Cactus*¹/*Carpets*² infrastructure (Schnetter et al. 2004) and the *AHFinderDirect* thorn (Thornburg 2004) to locate apparent horizons. This code has been extensively tested (Etienne et al. 2010) and used previously to study different scenarios involving compact binaries and B-fields (Etienne et al. 2012a,b). In all simulations, we use 9 levels of refinement with two sets of nested refinement boxes differing in size and resolution by factors of two. One set is centered on the NS and the other on the BH. The finest box around the BH (NS) has a half-side length $1.6 R_{\text{BH}}$ ($1.2 R_{\text{NS}}$). Here, R_{BH} (R_{NS}) is the initial BH (NS) radius. The finest levels resolve the BH (NS) radius by 30 (40) points. We set the outer boundary at $200M \simeq 1516(M_{\text{NS}}/1.4M_\odot)$ km, and impose reflection symmetry across the orbital plane.

The metric plus fluid initial data we use are identical to those in case B of Etienne et al. (2012b), and satisfy the conformal thin sandwich equations (see, e.g. Baumgarte & Shapiro 2010). The BH:NS mass ratio is 3 : 1. While the likely BHNS binary mass ratios may be closer to 7:1 (Belczynski et al. 2010), we choose 3:1 to compare with our earlier studies. Note that remnant disks from 7:1 mass ratio BH-NS mergers can have masses $\gtrsim 0.10M_\odot$, as obtained here, provided the initial black hole spin parameter is $\gtrsim 0.8$ (Foucart 2012). The initial NS is an irrotational, unmagnetized, $\Gamma = 2$ polytrope. Prior to tidal disruption, the magnetic field will be simply advected with (“frozen-into”) the fluid. To save computational resources and to avoid buildup of numerical errors, we evolve the system until two orbits prior to tidal disruption ($t = t_B$), at which point the NS is seeded with a dynamically weak, dipolar B-field generated by a vector potential A_ϕ approximating the vector potential of a current loop (see Eq. 2 in Paschalidis et al. 2013). We choose the loop current and radius such that in the interior the maximum value of the ratio of magnetic to gas pressure is $\beta^{-1} = 0.05$ which results in an interior B-field strength $B_{\text{int}} \simeq 10^{17}(1.4M_\odot/M_{\text{NS}})G$. While the resulting B-field strength is large, it is dynamically weak ($\beta^{-1} \ll 1$) and enables us to provide an “existence proof” for jet launching with the finite computational resources at our disposal. Specifically, we show that a NS endowed

with an initial dipolar magnetic field extending from its interior into the exterior enables magnetic launching of a jet following a BHNS merger. As this initial B-field is dynamically unimportant in the NS interior, we expect that the qualitative behavior obtained here will apply to other dynamically weak field choices.

To evolve the exterior B field reliably and also mimic the force-free conditions that likely characterize the exterior, at $t = t_B$ we impose a low but variable density atmosphere, as is typically done when evolving exterior B fields with ideal MHD codes. In particular, we construct an exterior in which the plasma parameter β initially is equal to some target value $\beta_0 < 1$ everywhere. This choice defines the NS surface as the place where the interior β falls to β_0 . For $\beta < \beta_0$ we are in the NS exterior and we reset the low exterior rest-mass density to $\rho_0 = \sqrt{0.5 \beta_0 b^2/K}$. Here, b^2 is the magnetic energy density, and $K = P/P_{\text{cold}}$ is the exterior ratio of gas pressure to cold pressure at $t = t_B$. The above prescription guarantees a universal $\beta = \beta_0$ in the exterior at $t = t_B$ and, at the same time, captures one key aspect of force-free electrodynamics, i.e., B-field pressure dominance. As the B-field strength falls from the NS surface as $1/r^3$, the above prescription forces ρ_0 to fall as $1/r^3$ as well. We note that our density prescription in the exterior is not enforced throughout the evolution. For the subsequent evolution, we evolve the density everywhere according to the ideal GRMHD equations imposing a density floor as is typically done in GRMHD codes. We vary $\beta_0 = 0.1, 0.05, 0.01$ to study exterior conditions ranging from partial to complete B-field pressure dominance, and check that the outcome remains invariant. For $\beta_0 = 0.01$ we have $b^2/\rho_0 \lesssim 1$ in the vicinity of the NS, and this case provides our best approximation to a force-free environment. As long as b^2/ρ_0 is not much larger than 1, our high-resolution-shock-capturing MHD code can handle the B-field evolution (see Duez et al. 2005; Etienne et al. 2010; Kiuchi et al. 2012). With our choice of β_0 the amount of total rest-mass does not increase by more than $\sim 1\%$, even for $\beta_0 = 0.1$. We also evolve the initial data without seeding any B fields, as well as repeating the calculation we performed in Etienne et al. (2012a) with initial poloidal B fields confined to the NS interior. We adopt a Γ -law EOS, allowing for shock heating.

All three β_0 cases with an external B field yield a magnetically driven, incipient jet, which is launched at $t_{\text{jet}} \sim 4000 - 6000M \simeq 100 - 150(M_{\text{NS}}/1.4M_\odot)$ ms after tidal disruption (depending on the value of β_0). We define an incipient, magnetized jet as an unbound, collimated, mildly relativistic outflow (Lorentz factor ~ 1.2), which is at least partially magnetically dominated. The outcome in all three β_0 cases satisfies the above definition. The time t_{jet} is also approximately the delay time between the peak GW amplitude and the jet onset.

3. RESULTS

As all of our cases demonstrate similar dynamics, we show snapshots only for $\beta_0 = 0.01$, the canonical case because the exterior pressure is well dominated by the B field while β_0 is within the range of what our code can treat reliably. Results for all cases are summarized in Table 1.

The merger and disk formation are displayed in Fig-

¹ <http://www.cactuscode.org/>

² <http://www.carpetscode.org/>

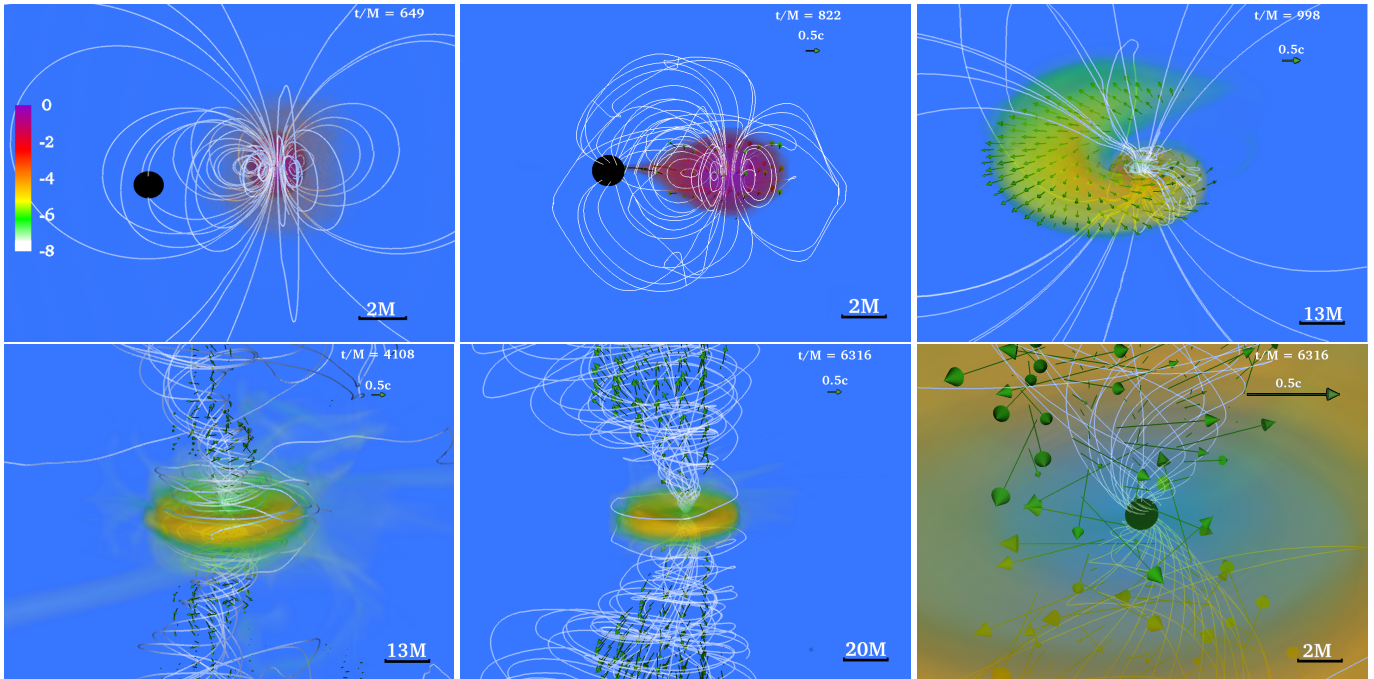


FIG. 1.— Snapshots of the rest-mass density, normalized to its initial maximum value $\rho_{0,\max} = 8.92 \times 10^{14} (1.4M_{\odot}/M_{\text{NS}})^2 \text{g cm}^{-3}$ (log scale), at selected times. Arrows indicate plasma velocities and white lines show the magnetic field lines. Bottom panels highlight the system after an incipient jet is launched. Here, $M = 2.5 \times 10^{-2} (M_{\text{NS}}/1.4M_{\odot}) \text{ms} = 7.58 (M_{\text{NS}}/1.4M_{\odot}) \text{km}$.

ure 1 and the dynamics are similar to what we reported in Etienne et al. (2012a,b) for case B, where the initial, purely poloidal B fields were confined to the NS interior. Following tidal disruption, a disk forms around a spinning BH with spin parameter $a/m \simeq 0.85$. The initial dynamically weak, dipolar B fields have little effect on the remnant disk rest-mass, which is $\sim 15\%$ of M_{NS} at $\sim 1000M \simeq 25(M_{\text{NS}}/1.4M_{\odot})\text{ms}$ after the time of peak accretion (at $t = t_{\text{acc}} = t_{\text{B}} + 300M$), as found in Etienne et al. (2009). The rest-mass accretion rate (\dot{M}), which we compute via Eq. A11 of Farris et al. (2010), begins to settle to an almost steady state at $t - t_{\text{acc}} \sim 2000M \simeq 50(M_{\text{NS}}/1.4M_{\odot})\text{ms}$, and subsequently decays slowly with time (see Figure 2). For $\beta_0 = 0.01$, when the outflow reaches $100\dot{M} = 758(M_{\text{NS}}/1.4M_{\odot})\text{km}$ above the BH poles, we find $\dot{M} = 0.25M_{\odot} \text{ s}^{-1}$ (see Table 1 for the other cases), at which time the disk mass is $\sim 0.13M_{\odot}(M_{\text{NS}}/1.4M_{\odot})$. Thus, the disk is expected to be accreted in $\Delta t \sim M_{\text{disk}}/\dot{M} \sim 0.5(M_{\text{NS}}/1.4M_{\odot})\text{s}$. It is interesting to note that the engine’s fuel – the disk – will be exhausted on a timescale entirely consistent with the typical duration of sGRBs: $T_{90} \sim 0.5\text{s}$ (see, e.g. Berger 2014), where T_{90} is the time over which 90% of the total counts of gamma-rays have been detected.

While we resolve the wavelength of the fastest growing magneto-rotational-instability (MRI) mode by at most five grid points, we see evidence for turbulent B fields in meridional slices of the disk. However, turbulence is not fully developed. Calculating the effective Shakura–Sunyaev α parameter associated with the magnetic stresses (as defined in Farris et al. 2012), we find that in the innermost $12M \simeq 91(M_{\text{NS}}/1.4M_{\odot})\text{km}$ of the disk and outside $\sim 5M \simeq 38(M_{\text{NS}}/1.4M_{\odot})\text{km}$ (the ISCO), α is 0.01 – 0.04 (see Table 1), indicating that accretion is likely driven by magnetic stresses. These

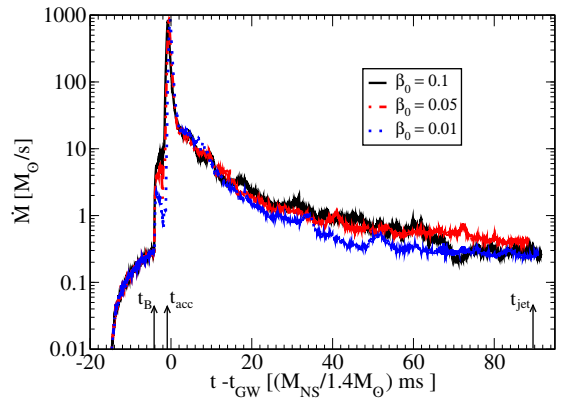


FIG. 2.— Rest-mass accretion rates for all cases in Table 1. Arrows indicate times t_{B} , t_{acc} , and t_{jet} for case $\beta_0 = 0.01$. Time is measured from the (retarded) time of the maximum GW amplitude, t_{GW} .

values of the effective α are similar to those found in other GRMHD simulations, including rapidly spinning BHs ($a/m \sim 0.9$) (Krolik & Hawley 2007) such as ours. Nevertheless, α may depend on resolution (Guan et al. 2009): higher resolution is required to accurately model the magnetically driven turbulence and hence to determine the precise lifetime of the remnant disk.

Neither the evolution without B field, nor the one with initial B field confined in the interior launch jets or show any evidence for an outflow. Instead, these runs exhibit inflows only, even when evolved for $5000M \simeq 125(M_{\text{NS}}/1.4M_{\odot})\text{ms}$.

While a predominantly toroidal B field is contained in the remnant disk, now the fluid elements inside the disk are linked via *exterior* B-field lines to other fluid elements in the disk and fluid elements that were pushed far away during tidal disruption. As a result, the B field outside the disk possesses a significant poloidal compo-

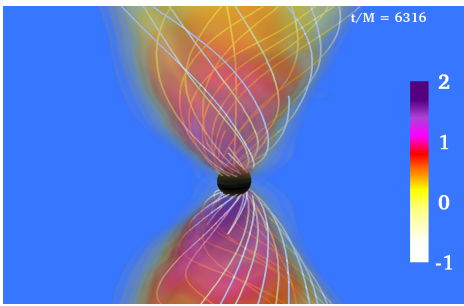


FIG. 3.— The ratio $b^2/2\rho_0$ (log scale) at $t-t_{acc} = 5316M$. White lines indicate the B-field lines plotted in the funnel where $b^2/2\rho_0 \geq 10^{-2}$. Magnetically-dominated areas ($b^2/\rho_0 \geq 1$) extend to heights greater than $15M \simeq 25r_{AH}$ above the BH horizon (shown as a black sphere). Here, $r_{AH} = 4.5(M_{NS}/1.4M_{\odot})\text{km}$ is the coordinate radius of the apparent horizon, which sets the length scale in the plot, and $M = 2.5 \times 10^{-2}(M_{NS}/1.4M_{\odot})\text{ms} = 7.58(M_{NS}/1.4M_{\odot})\text{km}$.

ment (see Figure 1). The angular velocity on 2D slices parallel to the orbital plane above the BH poles reveals that the fluid is differentially rotating. Therefore, following tidal disruption, magnetic winding of the plasma converts poloidal to toroidal flux (Shapiro 2000). This builds up the magnetic field above the BH poles until the environment becomes force-free, whereby the inflow is halted and eventually driven into an outflow collimated by the B field (see Figure 1). We find that above the BH poles, the comoving B field is amplified from $\sim 10^{13}(1.4M_{\odot}/M_{NS})\text{G}$ when the disk first settles to $\sim 10^{15}(1.4M_{\odot}/M_{NS})\text{G}$ when the incipient jet is launched.

In addition to differential rotation, the “footpoints” of the B-field lines above the BH poles have an associated angular frequency due to the Blandford-Znajek (BZ) effect (Blandford & Znajek 1977) once the environment becomes force-free (McKinney & Gammie 2004). As found in Komissarov (2001) for a monopole magnetic field around a BH with spin parameter $a/m = 0.9$ (close to the value of 0.85 of the BH remnant here), the ratio of the angular frequency of the B field ($\Omega_F = F_{t\theta}/F_{\theta\phi}$, where $F_{\mu\nu}$ is the Faraday tensor³) to the angular frequency of the BH [$\Omega_H = (a/m)/2m(1 + \sqrt{1 - (a/m)^2})$], increases from ~ 0.49 at the pole to ~ 0.53 near the equator. However, inside the jet funnel, where a force-free environment is approached, the B-field geometry is approximately paraboloidal. Thus, when the BZ effect operates, we expect that $\Omega_F/\Omega_H \sim 0.4 - 0.5$ within the funnel as the angle from the BH spin axis varies within 20 degrees (see Blandford & Znajek 1977; Yang et al. 2015). Hence, the B-field lines should rotate differentially. We computed Ω_F/Ω_H on an x - z slice passing through the BH centroid and along coordinate semicircles of radii r_{AH} and $2r_{AH}$, where r_{AH} is the BH apparent horizon radius, and find that $\Omega_F/\Omega_H \simeq 0.1 - 0.45$ within an opening angle of 20° from the BH rotation axis. Therefore, the BZ effect is likely operating, and the observed deviation of Ω_F/Ω_H from $\sim 0.4 - 0.5$ is probably due to deviations from strict stationarity and axisymmetry, the gauge required for our calculation of Ω_F , and possibly inadequate resolution. Values of $\Omega_F/\Omega_H \sim 0.45$ in the funnel

³ This formula is strictly correct for spacetimes that are stationary and axisymmetric and expressed in Killing coordinates, which is approximately true in our simulations at late times.

have been reported GRMHD accretion studies onto a single spinning BH with $a/m = 0.5$ (McKinney & Gammie 2004).

Following jet launching, the outflowing fluid elements in the asymptotically flat region have specific energy $E = -u_0 - 1 > 0$; hence, they are unbound. The characteristic maximum value of the Lorentz factor reached in the outflow is $\Gamma_L \sim 1.2$ (see Table 1). Thus, the incipient jet is only mildly relativistic. However, in the nearly force-free areas in the funnel, we find $b^2/2\rho_0 \sim 100$ (see Figure 3). For steady-state, axisymmetric Poynting-dominated jets, the maximum attainable Γ_L in the (asymptotic) jet is equal to the energy-to-mass flux ratio ($\simeq b^2/2\rho_0$) (Vlahakis & Königl 2003): incipient jets thus can be accelerated to $\Gamma_L \gtrsim 100$ as required by sGRB models. While baryon loading will generally hinder jet acceleration (see, e.g., Metzger et al. 2007) and limit the terminal Γ_L , the BZ effect alone, which we capture, can accelerate the jet to large Γ_L even in the presence of baryon contamination (McKinney 2005). Based on previous tests, the increase in the magnetization in the funnel is robust, but values of $b^2/2\rho_0$ exceeding 100 may not be reliable.

The level of collimation in the outflow is measured by the funnel opening angle. The boundary of the funnel area roughly coincides with the $b^2/2\rho_0 \simeq 10^{-2}$ contour. Based on this value, we estimate the typical opening angle of the incipient jets in all cases to be $\sim 20^\circ$ (see Figure 3).

To eliminate the possibility that the plasma in the jets originates from the artificial atmosphere only, we have tracked Lagrangian tracer particles and have found that most of the plasma replenishing the matter in the jet originates from the disk.

Computing the Poynting luminosity L_{EM} on the surface of a sphere of coordinate radius $r = 60M \simeq 455(M_{NS}/1.4M_{\odot})\text{km}$ (Etienne et al. 2012a) we find $L_{EM} \sim 10^{51}\text{ergs s}^{-1}$ (see Table 1), i.e., consistent with characteristic sGRB luminosities (Berger 2014). This value is also consistent with the EM power generated by the BZ effect: $L_{EM} \sim 10^{51}(a/m)^2(m/5.6M_{\odot})^2(B/10^{15}\text{G})^2\text{erg s}^{-1}$ (see, e.g. Eq. (4.50) in Thorne et al. 1986).

One of the main differences between the different β_0 cases is the time at which the jet is launched. This is expected: the higher β_0 , the larger the inertia of the atmospheric matter with respect to the B field, and the stronger the B field must become to overcome the ram pressure to launch a jet. Building up a stronger B field by winding requires more time, hence higher β_0 generally implies a delay in jet launching, which is consistent with our simulations.

4. CONCLUSIONS

We have shown that a NS in a BHNS system with an initially dynamically weak, dipolar B field launches an incipient jet (an unbound, collimated, mildly relativistic outflow) following tidal disruption. The accretion timescale of the remnant disk and energy output are consistent with those of typical sGRBs, demonstrating that the merger of BHNSs can indeed be the engines powering sGRBs. Although our results have been obtained with a high initial B field we expect that a smaller initial field will yield the same qualitative outcome. The reason is the following: The B field is dynamically weak in the

stellar interior and does not affect the tidal disruption, formation or structure of the disk. The amplification of the field following disruption is largely due to magnetic winding and MRI. These should combine to drive the field to values comparable to those found here since amplification proceeds until appreciable differential rotational and internal energy of the plasma, which is insensitive to the (weak) initial field, is converted to magnetic energy. This amplification should yield $B \sim 10^{15}$ G at the BH poles nearly independent of the initial NS B field, because BHNS simulations have shown that characteristic ambient densities following tidal disruption are $\sim 10^9 \text{ gr cm}^{-3}$ and magnetic launching is initiated when $b^2 \sim \rho_0 c^2$, yielding $b \sim 10^{15}$ G. Also, the amplification in the disk via MRI should not cease until the fields reach equipartition values: typical pressures in these disks of $P \sim \rho_0 v^2 \sim 10^{30} \text{ dyn cm}^{-2}$ should yield a magnetic field in the disk of $b \sim 10^{15}$ G. Winding occurs on an Alfvén timescale, so amplification may take longer the weaker the initial field. However, with the fields reaching comparable values to the one found here, the force-free exterior should drive a jet, and the BZ Poynting luminosity should be comparable to the values in Table 1, in agreement with observed sGRBs. We hope to investigate these

issues and confirm our expectations in future studies.

It is a pleasure to thank Zachariah Etienne, Charles Gammie, Roman Gold, and James Stone for helpful discussions. We also thank the Illinois Relativity group REU team (Sean E. Connelly, Abid Khan, and Lingyi Kong) for assistance in creating Figures 1 and 3, and R. Gold for sharing diagnostic 2D visualization software that helped in our analysis. This work has been supported in part by NSF grant PHY-1300903 and NASA grant NNX13AH44G at the University of Illinois at Urbana-Champaign. V.P. gratefully acknowledges support from a Fortner Fellowship at UIUC and support from the Simons foundation and NSF grant PHY-1305682. This work used the Extreme Science and Engineering Discovery Environment (XSEDE), which is supported by NSF grant number OCI-1053575. This research is part of the Blue Waters sustained-petascale computing project, which is supported by the National Science Foundation (award number OCI 07-25070) and the state of Illinois. Blue Waters is a joint effort of the University of Illinois at Urbana-Champaign and its National Center for Supercomputing Applications.

REFERENCES

- Acernese, F., & the VIRGO Collaboration. 2006, *Class. Quant. Grav.*, 23, S635
- Baumgarte, T., & Shapiro, S. 2010, *Numerical Relativity: Solving Einsteins Equations on the Computer* (Cambridge: Cambridge University Press)
- Beckwith, K., Hawley, J. F., & Krolik, J. H. 2008, *ApJ*, 678, 1180
- Belczynski, K., Dominik, M., Bulik, T., O’Shaughnessy, R., Fryer, C., & Holz, D. E. 2010, *ApJ*, 715, L138, 1004.0386
- Berger, E. 2014, *Ann. Rev. Astron. Astroph.*, 52, 43
- Blandford, R. D., & Znajek, R. L. 1977, *Mon. Not. Roy. Astron. Soc.*, 179, 433
- Brown, D. A., et al. 2004, *Class. Quant. Grav.*, 21, S1625
- Chawla, S., Anderson, M., Besselman, M., Lehner, L., Liebling, S. L., Motl, P. M., & Neilsen, D. 2010, *Physical Review Letters*, 105, 111101
- Deaton, M. B., Duez, M. D., Foucart, F., O’Connor, E., Ott, C. D., et al. 2013, *Astrophys.J.*, 776, 47
- Duez, M. D., Foucart, F., Kidder, L. E., Ott, C. D., & Teukolsky, S. A. 2010, *Class.Quant.Grav.*, 27, 114106
- Duez, M. D., Liu, Y. T., Shapiro, S. L., & Stephens, B. C. 2005, *Phys.Rev.*, D72, 024028
- East, W. E., Pretorius, F., & Stephens, B. C. 2012, *Phys. Rev. D*, 85, 124009
- Etienne, Z. B., Liu, Y. T., Paschalidis, V., & Shapiro, S. L. 2012a, *Phys.Rev.*, D85, 064029
- Etienne, Z. B., Liu, Y. T., & Shapiro, S. L. 2010, *Phys.Rev.*, D82, 084031
- Etienne, Z. B., Liu, Y. T., Shapiro, S. L., & Baumgarte, T. W. 2009, *Phys. Rev. D*, 79, 044024
- Etienne, Z. B., Paschalidis, V., & Shapiro, S. L. 2012b, *Phys.Rev.*, D86, 084026
- Farris, B. D., Gold, R., Paschalidis, V., Etienne, Z. B., & Shapiro, S. L. 2012, *Phys. Rev. Lett.*, 109, 221102
- Farris, B. D., Liu, Y. T., & Shapiro, S. L. 2010, *Phys.Rev.*, D81, 084008
- Foucart, F. 2012, *Phys. Rev. D*, 86, 124007, 1207.6304
- Foucart, F., Deaton, M. B., Duez, M. D., O’Connor, E., Ott, C. D., et al. 2014, *Phys.Rev.*, D90, 024026
- Guan, X., Gammie, C. F., Simon, J. B., & Johnson, B. M. 2009, *Ap. J.*, 694, 1010
- Kiuchi, K., Kyutoku, K., Sekiguchi, Y., Shibata, M., & Wada, T. 2014, *Phys.Rev.*, D90, 041502, 1407.2660
- Kiuchi, K., Kyutoku, K., & Shibata, M. 2012, *Phys. Rev. D*, 86, 064008
- Komissarov, S. S. 2001, *Mon. Not. Roy. Astron. Soc.*, 326, L41
- Krolik, J. H., & Hawley, J. F. 2007, in *American Institute of Physics Conference Series*, Vol. 924, *The Multicolored Landscape of Compact Objects and Their Explosive Origins*, ed. T. di Salvo, G. L. Israel, L. Piersant, L. Burderi, G. Matt, A. Tornambe, & M. T. Menna, 801–808, astro-ph/0611605
- Kuroda, K., & LCGT Collaboration. 2010, *Classical and Quantum Gravity*, 27, 084004
- Kyutoku, K., Ioka, K., & Shibata, M. 2013, *Phys.Rev.*, D88, 041503
- Lackey, B. D., Kyutoku, K., Shibata, M., Brady, P. R., & Friedman, J. L. 2014, *Phys.Rev.*, D89, 043009
- Lee, W. H., & Ramirez-Ruiz, E. 2007, *New Journal of Physics*, 9, 17, astro-ph/0701874
- Lovelace, G., Duez, M. D., Foucart, F., Kidder, L. E., Pfeiffer, H. P., et al. 2013, *Class.Quant.Grav.*, 30, 135004
- Lück, H., & the GEO600 collaboration. 2006, *Class. Quant. Grav.*, 23, S71
- McKinney, J. C. 2005, *ArXiv Astrophysics e-prints*, arXiv:astro-ph/0506368
- McKinney, J. C., & Gammie, C. F. 2004, *ApJ*, 611, 977
- Meszaros, P. 2006, *Rept.Prog.Phys.*, 69, 2259
- Metzger, B. D., Thompson, T. A., & Quataert, E. 2007, *ApJ*, 659, 561
- Pannarale, F., Berti, E., Kyutoku, K., & Shibata, M. 2013, *Phys.Rev.*, D88, 084011
- Paschalidis, V., Etienne, Z. B., & Shapiro, S. L. 2013, *Phys.Rev.*, D88, 021504
- Rezzolla, L., Giacomazzo, B., Baiotti, L., Granot, J., Kouveliotou, C., & Aloy, M. A. 2011, *ApJ*, 732, L6
- Schnetter, E., Hawley, S. H., & Hawke, I. 2004, *Class. Quantum Grav.*, 21, 1465, arXiv:gr-qc/0310042
- Shapiro, S. L. 2000, *Astrophys.J.*, 544, 397
- Shibata, M., & Taniguchi, K. 2011, *Living Reviews in Relativity*, 14, 6
- Tanaka, M., Hotokezaka, K., Kyutoku, K., Wanajo, S., Kiuchi, K., et al. 2014, *Astrophys.J.*, 780, 31
- Thornburg, J. 2004, *Class. Quant. Grav.*, 21, 743
- Thorne, K. S., Price, R. H., & Macdonald, D. A. 1986, *The Membrane Paradigm* (New Haven: Yale University Press)
- Vlahakis, N., & Königl, A. 2003, *ApJ*, 596, 1080
- Yang, H., Zhang, F., & Lehner, L. 2015, *ArXiv e-prints*, 1503.06788